

A two-way quantum interface for linking Sr^+ transition at 422nm to the telecommunications C-band

Thomas A. Wright^{1,*}, Robert J.A. Francis-Jones¹, Corin B.E. Gawith², Jonas N. Becker³, Patrick M. Ledingham³, Peter G.R. Smith², Joshua Nunn¹, Peter J. Mosley¹, Benjamin Brecht³, and Ian A. Walmsley³

¹Centre for Photonics and Photonic Materials, Department of Physics, University of Bath, Bath, BA2 7AY, UK

²Optoelectronics Research Centre, University of Southampton, SO17 1BJ, UK and

³Clarendon Laboratory, University of Oxford, Parks Road, Oxford, OX1 3PU, UK

(Dated: February 23, 2018)

We report a single-stage bi-directional interface capable of linking Sr^+ trapped ion qubits in a long-distance quantum network. Our interface converts photons between the Sr^+ emission wavelength at 422 nm and the telecoms C-band to enable low-loss transmission over optical fiber. We have achieved both up- and down-conversion at the single photon level with efficiencies of 9.4 % and 1.1 % respectively. Furthermore, we demonstrate that the noise introduced during the conversion process is sufficiently low to implement high-fidelity interconnects suitable for quantum networking.

Large scale quantum networks suitable for long-distance secure communication and distributed computation require not only that quantum information may be manipulated reliably, but also communicated successfully between remote nodes [1]. However, existing quantum information processing platforms are not individually able to fulfill both of these requirements. For example, photons can distribute quantum information through fiber networks [2] or via satellite [3] but multi-photon gates remain challenging, whereas trapped ions have achieved high-fidelity two-qubit operations [4] but are unsuitable for sharing entanglement beyond a single laboratory. However, integrating disparate technologies to form a hybrid light-matter quantum network promises the capability to carry out entanglement distribution and quantum communication over long distances [5].

The optical communication bus between nodes must overcome two technical challenges: compatibility between devices operating at different optical frequencies and low loss across large separations. Quantum frequency conversion (QFC), where a photon is coherently shifted to a different frequency band, addresses this difficulty by linking wavelengths as short as the ultraviolet (UV), where many convenient ion transitions are located, and the infrared (IR) telecommunications bands, enabling long-distance low-loss transmission in optical fiber [6].

QFC experiments initially focused on enhancing detection of IR photons by mapping them to the visible and near-infra-red (NIR) where efficient silicon photon detectors existed [7, 8]. The desire to improve transmission in fiber has motivated a continuation of QFC experiments translating photons both from [9–15] and to [16–20] different telecommunication bands, though in large these have exploited opportune laser wavelengths and transitions predominantly in the red and NIR. Recently, translation between ultraviolet and the O-band has been shown [21, 22], albeit only in one direction.

Further reports of one way frequency conversion between node wavelengths have also been made [23–28]. Additionally, near-unit efficiency QFC has been demonstrated [29], though only over a small frequency shift, with similar approaches to larger frequency jumps yielding lower conversion efficiency [30]. The majority of reported conversions thus far have been unidirectional, whereas to create a functional quantum network in fiber, shifting to the telecoms is critical and two-way conversion is desirable.

We report the realization of single stage bi-directional frequency conversion at the single photon level for interfacing the $\text{S}_{1/2} \rightarrow \text{P}_{1/2}$ transition in trapped Sr^+ ion qubits (422 nm) with the telecommunications C-band (1550 nm). The conversion is achieved in a magnesium-doped periodically poled lithium niobate (MgO:PPLN) crystal, where $\chi^{(2)}$ sum or difference frequency generation (SFG or DFG) can be used to achieve up or down conversion of an input photon. We demonstrate that the noise level, expressed as the mean input photon number that would result in a signal-to-noise ratio of 1, μ_1 [31], is as low as 0.0185 – far below the level required for use as the interface in a hybrid quantum network. This is to our knowledge the lowest-noise performance reported to date, and the only bi-directional link between blue ion transitions and the C-band.

In order to map the input to the target output wavelength, a strong pump field must be tuned to fulfill the energy conservation requirement $\hbar\omega_{in} + \hbar\omega_{pump} = \hbar\omega_{out}$ for SFG up conversion and $\hbar\omega_{in} - \hbar\omega_{pump} = \hbar\omega_{out}$ for DFG down conversion. In both SFG and DFG the amplitude of the strong pump serves to drive the nonlinear optical response facilitating the conversion. The efficiency of the process is related to the strength of the coupling between the fields in the QFC Hamiltonian:

$$\hat{\mathcal{H}} = i\hbar\kappa A_{pump} (\hat{a}_{out}^\dagger \hat{a}_{in} - h.c.) \quad (1)$$

determined by the parameter κ , which itself is dependent on the magnitude of the fields but also on their relative phase, spatial overlap in the crystal and a the intrinsic nonlinearity of the material [6].

* t.wright@bath.ac.uk

For such widely-separated wavelengths, the large wave-vector mismatch Δk between the propagation constants of the three fields means that phase matching is difficult to satisfy in commonly-available materials. Even typical quasi phase matched (QPM) crystals that achieve efficient conversion when

$$\Delta k = k_{out} - k_{in} - k_{pump} - \frac{2\pi}{\Lambda} = 0, \quad (2)$$

have a poling pitch Λ that is too long to compensate the large Δk in our interaction. Hence, we used a MgO:PPLN crystal fabricated in collaboration with Coversion Ltd with ferroelectric domains created using a proprietary electric field poling technique to produce a very short pitch. A photoresist pattern was created on the $-z$ (bottom) face of a 0.5 mm-thick single-domain z -cut 3 inch diameter MgO:LiNbO₃ crystal wafer. Liquid electrodes were applied to both the patterned z and unpatterned $+z$ surfaces of the crystal to enable electrical contact with the wafer surface. Domain inversion along the z -axis was performed at room temperature by voltage-controlled application of electric field based on a first stage of domain nucleation above the coercive field of the crystal, and a second stage of domain spreading near the coercive field ($\sim 4.5 \text{ kV mm}^{-1}$); this technique results in inverted domains that traverse the entire thickness of the crystal. The MgO:PPLN wafer was diced and polished into multiple chips, each containing five 300 μm -wide gratings with periods of 3.75, 3.85, 3.95, 4.05, and 4.15 μm respectively. These periods were calculated to enable SFG and DFG processes between 422 nm and the telecoms C-band. The MgO:PPLN crystal used in this experiment was 19.97 mm long, with the 3.75 μm grating selected; it was not anti-reflection coated.

The experimental setup for characterizing the SFG up conversion is shown in Fig. 2(a). An 80 MHz synchronously pumped tunable dye laser operating at 580 nm wavelength and 30 ps pulse duration (Sirah Gropius) was used to pump the conversion and a tunable continuous-wave (CW) laser with a 40 MHz linewidth (Santec TSL-510 C), provided a coherent IR input that was attenuated to low mean photon number. The pump and input beam size and polarization were set using telescopes and half wave plates (HWPs) before the beams were combined at a dichroic mirror (DM) and directed towards the MgO:PPLN crystal. A pair of fused silica lenses were then used to focus the overlapped beams in to the crystal. Care was taken to balance matching the Rayleigh length of each beam to half the crystal length while minimizing the difference between the cross-sections of the beam waists. Following the crystal, a flipper mirror allowed for the input and pump powers transmitted through the crystal to be measured. The pump, unconverted IR input light and successfully converted violet output were then separated using a series of dichroic and short pass (SPF) filters before being directed to two single-photon avalanche diodes (SPADs). At the short wavelength, the pump light was removed

using short pass filters at 500 nm and 440 nm as well as a short-pass dichroic filter with an edge at 500 nm. The remaining signal was monitored by a blue-enhanced Si SPAD with a detection efficiency and dark count rate of 86 % and 6 Hz. For the long wavelength we utilized a fiber-coupled InGaAs SPAD operating at 9.5 % detection efficiency. A spectrograph with electron-multiplying CCD camera was available to monitor the spectra.

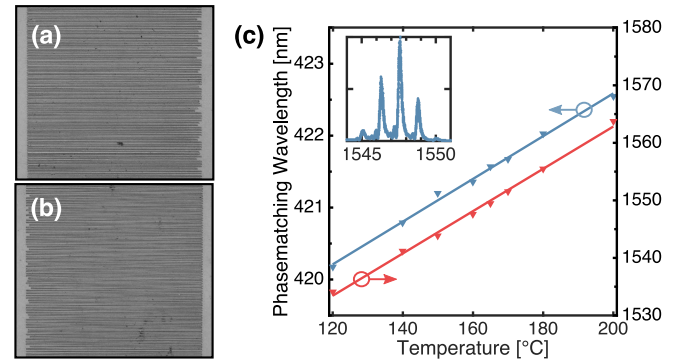


FIG. 1. Optical micrographs of the (a) $+z$ (top) and (b) $-z$ (bottom) surface of one of the 3.75 μm periodically poled MgO:LiNbO₃ crystals. (c) Phase-matching characteristics. The temperature response of the phase-matching of the 3.75 μm poled crystal, i.e., the wavelength of perfect phase matching as a function of crystal temperature. *Inset* SFG phase-matching curve, i.e., short wavelength output power as a function of input telecom wavelength at constant crystal temperature and pump power.

In order to maximize the coupling constant, κ , the phase matching of the crystal was first characterized. With the temperature of the crystal stabilized at 160°C, the input IR beam was swept in wavelength whilst the intensity of the converted violet light was measured, mapping out the phase matching curve, for a pump wavelength of 579.6 nm. We observed several distinct peaks in the phase matching (see Fig. 1), indicative of either multiple frequency modes within the pump beam or inhomogeneous poling across the length of the crystal.

We measured the change in position of the central phase matching peak as a function of temperature, for a range of crystal temperatures by sweeping the input wavelength whilst measuring the output violet power using an amplified photodiode. For the input IR light we measured a temperature response of $\Delta\lambda_{in}/\Delta T = 0.4 \text{ nm/K}$, corresponding to the a change in the output wavelength of $\Delta\lambda_{out}/\Delta T = 0.0297 \text{ nm/K}$.

Having established the phase matching response of the crystal, we investigated the achievable up conversion efficiency. IR light at 1547.6 nm was converted to 421.7 nm by pumping the process at 579.6 nm with a fixed crystal oven temperature of 160°C.

We present the external efficiency, η_{ext} , of the SFG conversion in Fig. 2(b), which we define as the mean number of converted photons leaving the crystal divided by the number of input photons incident and temporally

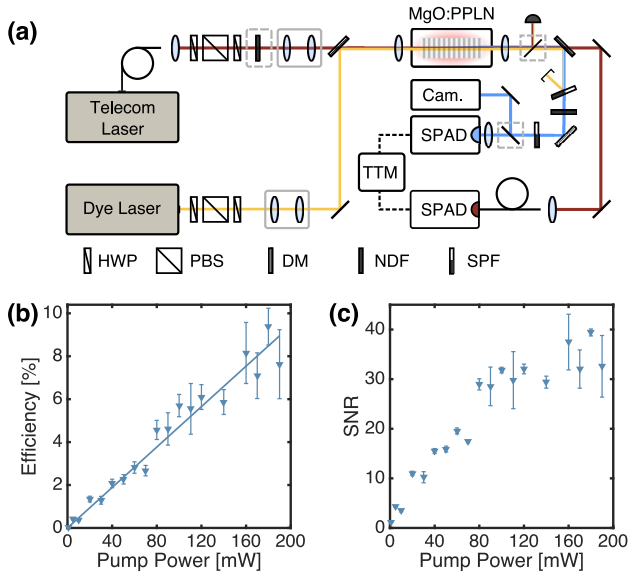


FIG. 2. (a) Experimental setup of the SFG up conversion. (b) Up conversion efficiency of the interface. (c) Signal-to-noise ratio of the up conversion.

overlapped with the pump. The number of input photons, $\langle n \rangle_{in}$, is therefore given by

$$\langle n \rangle_{in} = (P_{in} \cdot D) / (\hbar\omega_{in}), \quad (3)$$

where P_{in} was measured as the input power transmitted through the crystal. Due to observations of drift in the IR input power, this was measured both before and after each integration over which we recorded detector counts and used to calibrate the continuous monitoring of the IR light at SPAD detector 2. Due to the CW nature of the input light, the duty cycle D was defined as the pump pulse width divided by the inverse of the repetition rate: $D = \tau_{pump} \cdot R_p$.

The conversion efficiency was then calculated as

$$\eta_{ext} = (S - N) / (\langle n \rangle_{in} \cdot \eta_{loss}), \quad (4)$$

where S and N are the signal and noise respectively. η_{loss} incorporates the detector efficiency ($\sim 86\%$), transmission through optical components ($\sim 96\%$) and, at higher powers, a neutral density filter (NDF) used to prevent detector saturation ($\sim 20\%$).

In order to demonstrate the capability of the interface to operate at low photon numbers we set a target input of overlapping an average of two IR photons with every pump pulse. The resulting conversion efficiency is shown in Figure 2(b). The highest measured external efficiency of $\eta_{ext} = 9.4 \pm 0.86\%$ was observed for an average pump power of 180 mW. Each point in Figure 2(b) corresponds to a measurement consisting of between 5 and 10 s of integration, beyond which we observed a drop in efficiency. This was later realized to be due to absorption of the pump light causing localized heating of the crystal, resulting in a change in the phase matching. The phenomena of pump power induced change in Δk for $\chi^{(2)}$ QFC

processes has been discussed previously [22, 32]. Additional change in the phase mismatch is also introduced due to the photorefractive effect and as such, when operating over extended periods of time as would be required in a network, the process would be pumped at a constant power, with the phase matching temperature tuning being optimized at the selected pump power.

Figure 2(c) shows the signal to noise ratio (SNR) achieved across a range of pump powers, where we define $SNR = S/N$. The SNR achieved for the point at which we achieved highest conversion was 39.4 ± 0.69 . The main source of noise was pump light leaking through the filters to the detector, which can, in principle, be easily removed.

In order to demonstrate a two way interface, we similarly characterized the reverse process, converting single-photon level violet light to IR via DFG. Figure 3(a) shows the modified experimental setup. The input light at 425.5 nm was obtained by second harmonic generation of a 80 MHz repetition rate Ti:sapphire laser operating at 851 nm wavelength and 300 ps pulse duration (Spectra Physics Tsunami) which was synchronized to the clock signal of the dye laser system via active cavity-length control. Replicating the interface between 421.7 nm and the C-band was not possible due to the phase matching restriction of the SHG crystal. In order to successfully translate the violet light to the telecoms C band we tuned the wavelength of the dye laser to 585 nm and adjusted the crystal oven temperature to 226.4°C. This enabled us to optimize conversion to 1560.6 nm. Mitigation of the pump induced change in $\Delta\beta$ was achieved by optimizing the oven temperature whilst pumping the nonlinear conversion with an average power of 60 mW, half of the available range. In the long wavelength detection arm the filtering consisted of two long pass filters with edges at 950 and 650 nm. A 8.9 nm-wide band pass filter was used, centered at 1570 nm and rotated in order to shift the transmission to accommodate the converted light at 1560 nm.

In Fig. 3(b) we present the external efficiency of the conversion, where we have accounted for sources of loss outside the crystal, as described by Eq. 3. We evaluated η_{loss} , incorporating the detector efficiency ($\sim 9.5\%$), transmission through optical components ($\sim 73\%$) and fiber coupling efficiency ($\sim 65\%$). The duty cycle D was defined as the ratio of the pump and input pulse durations: $D = \tau_{pump} / \tau_{input}$. The same target input photon number as the SFG conversion, of $\langle n \rangle = 2$, was used in the DFG experiment. Across the data collected, counts were measured for integration times longer than 15 s.

The pump and input beam were steered using mirrors ahead of the crystal to the optimize beam overlap leading to a wide distribution of observed conversion at comparable pump powers. A maximum external conversion efficiency of $1.1 \pm 0.12\%$ was achieved for a pump power of 120 mW, while significantly lower than the $\sim 6\%$ external efficiency observed for the SFG at equal pump power,

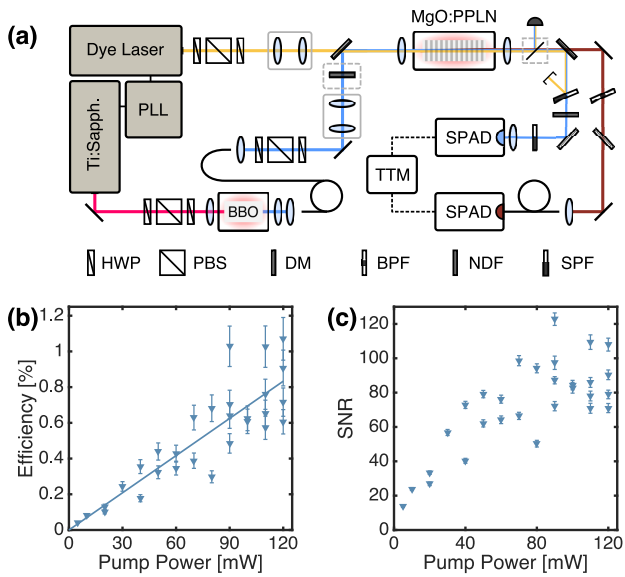


FIG. 3. (a) Experimental setup of the DFG down conversion. (b) Down conversion efficiency of the interface. (c) Signal-to-noise ratio of the down conversion.

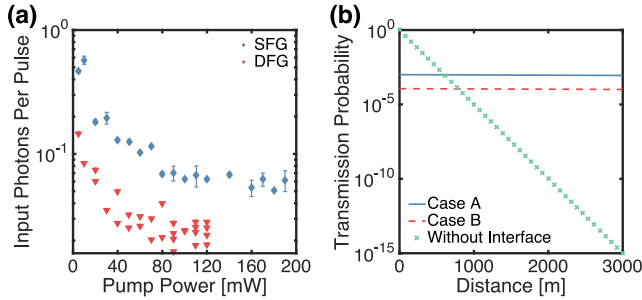


FIG. 4. (a) μ_1 , The lowest number of photons per pulse possible to send into the device to get an $\text{SNR} \geq 1$. (b) Probability of successful transmission of two photons from remote trapped Sr^+ ion processing nodes to an entangler along a fiber network with and without our interface.

may be partly accounted for by a change in beam waist between the two experiments. The beam waist of the pump in both experiments was $\sim 43.2 \mu\text{m}$, while the input light beam waist was increased from $\sim 63.3 \mu\text{m}$ in the SFG up conversion to $\sim 112 \mu\text{m}$ in the DFG down conversion. This would indicate that the maximum proportion of the input overlapped by the pump changed from $\sim 46.6\%$ to $\sim 14.9\%$. It could be expected that further optimization of optics selection may yield improved conversion efficiencies, in particular when considered for the DFG down-conversion. Again, we draw attention to the conversion efficiency being limited by the available pump power in the experiment, as can be seen from the linear slope of the efficiency vs pump power curve in Fig. 3(b).

The down conversion was shown to be low noise in operation, with a SNR of 108 ± 3.8 measured at the point of highest conversion. A large contributing factor to the higher SNR in the down conversion was due to the IR de-

tector's lack of sensitivity at the pump light wavelength, largely eliminating pump leakage as a source of noise. This demonstrates that there is next to no noise from spurious parametric down-conversion, a typical noise process in interfaces linking short and long wavelengths [22].

In order to demonstrate that our device is capable of operating as a QFC interface in a quantum network, for both up and down conversion, we calculated the mean input photon number per pulse that would yield a $\text{SNR} = 1$, commonly referred to as μ_1 [31]. Originally defined for quantum memories, the parameter μ_1 provides a useful performance benchmark for frequency conversion as it normalizes the noise by the conversion efficiency, thus precluding noise reduction by pumping with unrealistically low power. The calculated values are shown in Figure 4(a). For the up conversion we found the minimum $\mu_1 = 0.05074$ when operating at a pump power of 180 mW. We note that this value was limited by the pump power in the experiment, as can be seen from the linear slope of the efficiency vs pump power curve. For the down conversion, at a pump power of 120 mW, μ_1 to be 0.0185. Hence we see that noise photons originating from intrinsic spontaneous parametric down conversion of the pump field – typically a limiting factor in $\chi^{(2)}$ QFC schemes – do not cause significant detrimental effects in our system. The values of $\mu_1 \ll 1$ demonstrate that low-noise operation can be maintained while using broadband spectral filtering, rather than high loss narrow band filters, making our device suitable for integration in to a real world network.

In Figure 4(b) we consider the end-to-end efficiency of three scenarios in which entanglement needs to be established between remote processing nodes, taking into account the transmission loss of fiber at the wavelengths 422 nm and 1550 nm ($<50 \text{ dB/km}$ for SM400 at 422 nm and $<0.18 \text{ dB/km}$ for SMF-28 at 1550 nm). In case A a violet photon from node 1 is down-converted via our interface and transmitted through a length of optical fiber before reaching the location of the second node, where it is up-converted to allow interference with a photon emitted directly from the node 2. In case B both photons emitted by the ion traps are down-converted before being transmitted through optical fiber and interfered at some midway position. The final case is where no interface is used and a violet photon is emitted from one of the nodes before being transmitted through fiber to the second node whereupon an entanglement link is established. For each case we present the probability of the photons successfully reaching their destination, assuming no coupling loss. We see that the use of our interface would drastically increase the probability of successful end-to-end transmission for remote nodes linked by fiber.

In conclusion, we have implemented a QFC interface capable of low noise up- and down-conversion of single-photon-level light with efficiencies of 9.4 % and 1.1 % respectively in a custom-poled MgO:PPLN crystal. When considering the transmission loss of single mode fiber at the Sr^+ emission wavelength of 422 nm relative to that

at 1550 nm, our interface would increase the probability of successful transmission of quantum information by 47 orders of magnitude over a distance of 10 km. We have demonstrated that the noise introduced by our QFC interface is far below the level required to achieve high-fidelity conversion of single photons emitted by trapped Sr^+ ions. Hence we believe that our interface will enable long-distance entanglement distribution through chains of nodes containing trapped Sr^+ ions, paving the way to

the construction of large-scale quantum networks.

This work was funded by the UK EPSRC Quantum Technology Hub Networked Quantum Information Technologies, grant number EP/M013243/1. BB acknowledges funding from the European Unions (EU) Horizon 2020 research and innovation program under Grant Agreement No. 665148. PML acknowledges funding from the European Union Horizon 2020 Research and Innovation Framework Programme Marie Curie individual fellowship, Grant Agreement No. 705278.

[1] L. M. Duan, M. D. Lukin, J. I. Cirac, and P. Zoller, *Nature* **414**, 413 EP (2001).

[2] Q.-C. Sun, Y.-F. Jiang, Y.-L. Mao, L.-X. You, W. Zhang, W.-J. Zhang, X. Jiang, T.-Y. Chen, H. Li, Y.-D. Huang, X.-F. Chen, Z. Wang, J. Fan, Q. Zhang, and J.-W. Pan, *Optica* **4**, 1214 (2017).

[3] J. Yin, Y. Cao, Y.-H. Li, J.-G. Ren, S.-K. Liao, L. Zhang, W.-Q. Cai, W.-Y. Liu, B. Li, H. Dai, M. Li, Y.-M. Huang, L. Deng, L. Li, Q. Zhang, N.-L. Liu, Y.-A. Chen, C.-Y. Lu, R. Shu, C.-Z. Peng, J.-Y. Wang, and J.-W. Pan, *Physical Review Letters* **119**, 200501 (2017).

[4] C. J. Ballance, T. P. Harty, N. M. Linke, M. A. Sepiol, and D. M. Lucas, *Physical Review Letters* **117**, 060504 (2016).

[5] R. Nigmatullin, C. J. Ballance, N. d. Beaudrap, and S. C. Benjamin, *New Journal of ...* **18**, 103028 (2016).

[6] P. Kumar, *Optics letters* **15**, 1476 (1990).

[7] M. A. Albota and F. N. C. Wong, *Optics letters* **29**, 1449 (2004).

[8] A. P. Vandevender and P. G. Kwiat, *Journal of Modern Optics* **51**, 1433 (2004).

[9] S. Tanzilli, W. Tittel, M. Halder, O. Alibart, P. Baldi, N. Gisin, and H. Zbinden, *Nature* **437**, 116 (2005).

[10] A. P. Vandevender and P. G. Kwiat, *JOSA B* **24**, 295 (2007).

[11] T. Honjo, H. Takesue, H. Kamada, Y. Nishida, O. Tadanaga, M. Asobe, and K. Inoue, *Optics express* **15**, 13957 (2007).

[12] M. T. Rakher, L. Ma, O. Slattery, X. Tang, and K. Srinivasan, *Nature Photonics* **4**, 786 (2010).

[13] M. T. Rakher, L. Ma, M. Davanco, O. Slattery, X. Tang, and K. Srinivasan, *Physical Review Letters* **107**, 083602 (2011).

[14] C. E. Vollmer, C. Baune, A. Sambrowski, T. Eberle, V. Händchen, J. Fiurášek, and R. Schnabel, *Physical Review Letters* **112**, 073602 (2014).

[15] C. Baune, J. Gniešmer, S. Kocsis, C. E. Vollmer, P. Zell, J. Fiurášek, and R. Schnabel, *Physical Review A* **93**, 010302 (2016).

[16] R. Ikuta, Y. Kusaka, T. Kitano, H. Kato, T. Yamamoto, M. Koashi, and N. Imoto, *Nature Communications* **2**, 1544 (2011).

[17] S. Zaske, A. Lenhard, C. A. Kessler, J. Kettler, C. Hepp, C. Arend, R. Albrecht, W.-M. Schulz, M. Jetter, P. Michler, and C. Becher, *Physical Review Letters* **109**, 147404 (2012).

[18] K. De Greve, L. Yu, P. L. McMahon, J. S. Pelc, C. M. Natarajan, N. Y. Kim, E. Abe, S. Maier, C. Schneider, M. Kamp, S. Höfling, R. H. Hadfield, A. Forchel, M. M. Fejer, and Y. Yamamoto, *Nature* **491**, 421 EP (2012).

[19] J. S. Pelc, L. Yu, K. De Greve, P. L. McMahon, C. M. Natarajan, V. Esfandyarpour, S. Maier, C. Schneider, M. Kamp, S. Höfling, R. H. Hadfield, A. Forchel, Y. Yamamoto, and M. M. Fejer, *Optics express* **20**, 27510 (2012).

[20] B. Albrecht, P. Farrera, X. Fernandez-Gonzalvo, M. Cristiani, and H. de Riedmatten, *Nature Communications* **5**, 3376 (2014).

[21] H. Rütz, K.-H. Luo, H. Suche, and C. Silberhorn, *Applied Physics B* **122**, 13 (2016).

[22] H. Rütz, K.-H. Luo, H. Suche, and C. Silberhorn, *Phys. Rev. Applied* **7**, 024021 (2017).

[23] V. Krutyanskiy, M. Meraner, J. Schupp, and B. P. Lanyon, *Applied Physics B* **123** (2017), 10.1007/s00340-017-6806-8.

[24] N. Maring, P. Farrera, K. Kutluer, M. Mazzera, G. Heinze, and H. de Riedmatten, *Nature* **551**, 485 (2017).

[25] M. Bock, P. Eich, S. Kucera, M. Kreis, A. Lenhard, C. Becher, and J. Eschner, *arXiv.org* (2017), 1710.04866v1.

[26] T. Walker, K. Miyanishi, R. Ikuta, H. Takahashi, S. V. Kashanian, Y. Tsujimoto, K. Hayasaka, T. Yamamoto, N. Imoto, and M. Keller, *arXiv.org* (2017), 1711.09644v2.

[27] J. D. Siversn, J. Hannegan, and Q. Quraishi, *arXiv.org* (2018), 1801.01193v1.

[28] A. Dréau, A. Tchekhovateva, A. El Mahdaoui, C. Bonato, and R. Hanson, *arXiv.org* (2018), 1801.03304v1.

[29] A. S. Clark, S. Shahnia, M. J. Collins, C. Xiong, and B. J. Eggleton, *Optics letters* **38**, 947 (2013).

[30] H. J. McGuinness, M. G. Raymer, C. J. McKinstry, and S. Radic, *Physical Review Letters* **105**, 093604 (2010).

[31] M. Gündoğan, P. M. Ledingham, K. Kutluer, M. Mazzera, and H. de Riedmatten, *Physical Review Letters* **114**, 230501 (2015).

[32] O. A. Louchev, N. E. Yu, S. Kurimura, and K. Kitamura, *Applied Physics Letters* **87** (2005), 10.1063/1.2056593.